Supporting information

The Structure of the Mercury Transporter MerF in Phospholipid Bilayers: A Large Conformational Rearrangement Results From N-terminal Truncation

George J. Lu†, Ye Tian†,‡, Nemil Vora†, Francesca M. Marassi‡ and Stanley J. Opella*,†

† Department of Chemistry and Biochemistry, University of California, San Diego, La Jolla, California, 92093-0307

‡ Sanford-Burnham Medical Research Institute, La Jolla, California 92037, United States

Protein Expression and Purification. The expression and purification of MerF followed previously described protocols used for similar proteins[1-5]. The gene encoding the full-length construct of MerF was cloned into an *E. coli* pET31b+ vector (Novagen, www.emdmillipore.com) for expression of a KSI-MerF-His_6 fusion protein with the three polypeptide segments separated by methionine residues. The fusion protein was expressed in *E. coli* C41(DE3) cells (Lucigen, www.lucigen.com) in M9 minimal medium containing 1 g/L ^{15}N labeled ammonium sulfate (Cambridge Isotope Laboratories (CIL), www.isotope.com) as the sole nitrogen source, 2-3 g/L of $^{13}C_6$-glucose (CIL) as the sole carbon source, 50 mg/L of carbenicillin as the antibiotic. The cell cultures were grown by shaking (250 rpm) at 37°C until the OD_{600} reached 0.6. Expression of the fusion protein was induced by adding 1 mM IPTG and growing for an additional 3-5 hr. Cells were harvested by centrifugation, resuspended in 60 ml lysis buffer (20 mM Tris-HCl, 500 mM NaCl, 15% glycerol, pH 8.0) per liter of cell culture, and lysed by a probe sonicator (Fisher Scientific Sonic Dismembrator 550, www.fishersci.com) on ice. The inclusion bodies containing the fusion protein were separated by centrifugation at 13,000 rpm (JA-20 rotor, Beckman Coulter, www.beckmancentrifuge.com), and then solubilized in the binding buffer (20 mM Tris-HCl, 500 mM NaCl, 6 M guanidine hydrochloride, 5 mM imidazole, pH 8.0). Following a 30-minute centrifugation at 17,000 rpm, the supernatant was separated and allowed to bind Ni-NTA agarose (Qiagen, www.qiagen.com) beads in a column pre-equilibrated with binding buffer. The column was then washed with washing buffer (20 mM Tris-HCl, 500 mM NaCl, 6 M guanidine hydrochloride, 50 mM imidazole, pH 8.0), and the fusion proteins were eluted with elution buffer (20 mM Tris-HCl, 500 mM NaCl, 6 M guanidine hydrochloride, 500 mM imidazole, pH 8.0). The polypeptides were then dialyzed extensively in water and lyophilized. The polypeptides were resolubilized in 70% formic acid, and then cleaved for 5 hours in the presence of excess of cyanogen bromide and the absence of light. The reaction was terminated by adding two volumes of 1 M NaOH; the polypeptides were then dialyzed and lyophilized. Isotopically labeled MerF was further purified by reverse-phase HPLC (DeltaPak C4 Column, Waters, www.waters.com).

Proteoliposome Reconstitution. 20 mg of 1,2-di-O-tetradecyl-*sn*-glycero-3-phosphocholine (14-o-PC) powder (Avanti Polar Lipids, www.avantilipids.com) and 4 mg of MerF were separately dissolved in solutions containing 1% SDS and 20 mM MES, pH 6.1. The two solutions were mixed with gentle shaking for 1 hour. The removal of SDS follows the protocol previously described[6,7]. The bulk of the SDS was removed by dialyzing the solution for 24 hours against >100 fold excess volume of 20 mM MES buffer, pH 6.1. The solution was dialyzed again for 8-12 hours against a >100 fold excess volume of 20 mM MES buffer, pH 6.1 with 10 mM KCl. A third dialysis repeated using the conditions of the first one to remove residual KCl and SDS.

NMR sample preparation. MerF-containing proteoliposomes were concentrated by ultracentrifugation (390,000 g, Beckman Ti 70.1 rotor, overnight, 15°C, www.beckmancentrifuge.com) and the pellet was packed into the 3.2mm MAS rotor for NMR studies.

NMR Experiments. The NMR experiments and associated parameters are described in Supplementary Table 1. The experimental NMR data were processed and analyzed using NMRPipe[8] and Sparky[9]. ^{1}H decoupling was achieved with SPINAL-64[10]. ^{13}C-^{13}C correlation was achieved with proton-driven spin diffusion (PDSD)[11,12] or dipolar assisted rotational resonance (DARR)[13]. Multiple-contact cross polarization[14,15] was implemented for magnetization transfer between ^{1}H and $^{15}N/^{13}C$. The magnetization transfer between ^{15}N and $^{13}C\alpha$ or $^{13}C'$ was performed using SPECIFIC-CP[16]. Heteronuclear dipolar recoupling was performed using the $R18^{7}_{1}$ sequence[17-19].

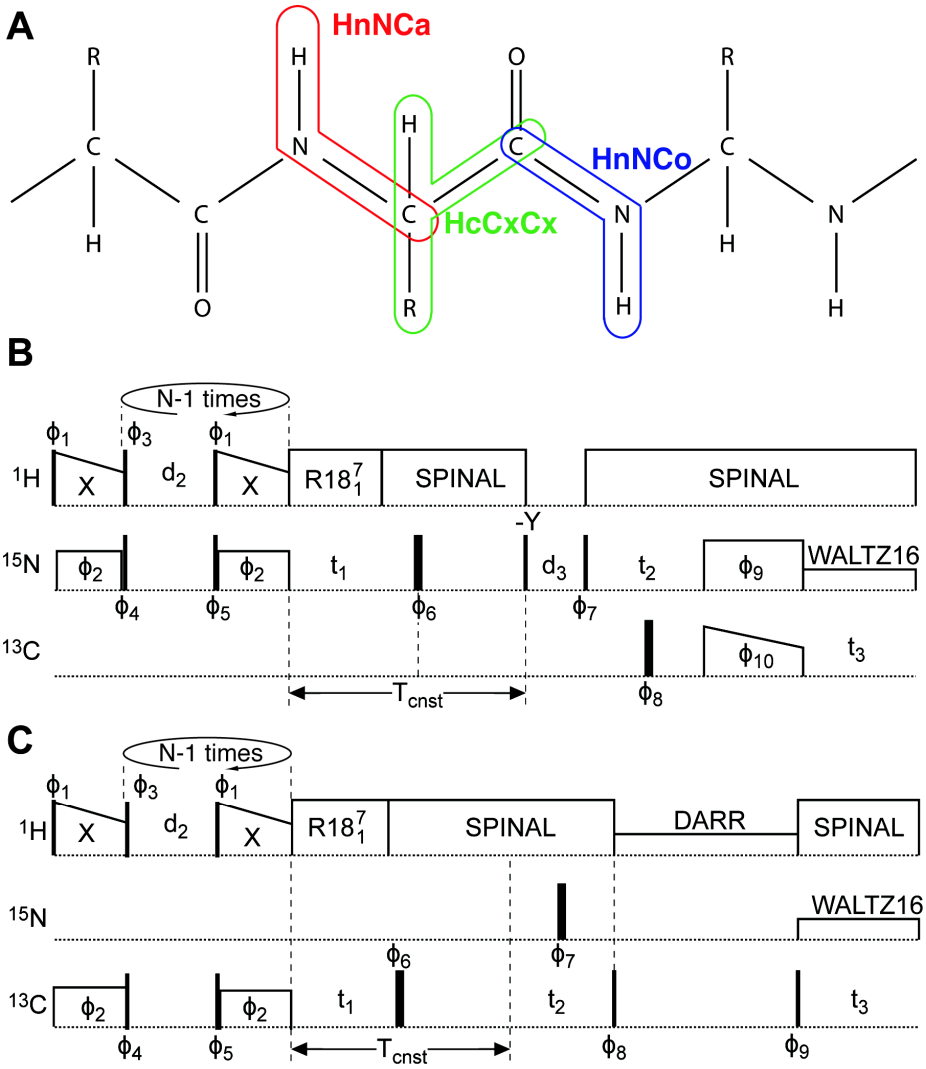

Supplementary Figure 1. A. Schematic drawing of a polypeptide outlines the atoms in the coupling pathways utilized in the NMR experiments. B. and C. The timing diagrams for the three three-dimensional experiments used to make resonance assignments and measure the frequencies that provided the angular restraints for structure determination. The inclusion of one dipolar coupling dimension in each of the experiments increases the resolution of the spectra, and it is especially important for discerning the assignments among the same types of amino acids, since their ^{13}Cα, ^{13}C' and amide ^{15}N atoms typically have similar chemical shift frequencies. The use of these experiments combines the resonance assignments and dipolar coupling measurements in a single step, reducing the total number of three-dimensional experiments that are required. B. The pulse sequence for HnNCa and HnNCo experiments with ^{1}H-^{15}N multiple-contact cross polarization. C. The pulse sequence for the HcCxCx experiment with ^{1}H-^{13}C multiple-contact cross polarization.

Supplementary Table 1. NMR experiments and parameters[a].

Two-dimensional ^{13}C-^{13}C Correlation	**short-range**	**long-range**
MAS spinning speed (Hz)	11111	11111
mixing time [ms]	50 (PDSD)	200 (DARR)
acquisition time (t2/t1) [ms]	10/6.56	12.9/6.56
carrier frequency (t2/t1) [ppm]	100/40	100/40
π/2 pulse ($^{1}H/^{13}C$) [μs]	2.7/4.7	2.7/4.7
CP contact time [μs]	200	200
CP pulse shape (^{1}H)	Linear (100-80%)	Linear (100-80%)
CP rf field strength ($^{1}H/^{13}C$) [kHz]	66/55	66/55
^{1}H decoupling field strength (sw-TPPM) [kHz]	100	100
recycle delay [s]/number of acquisitions	2/896	2/2240
spectral width (F2/F1) [kHz]	39.68/12.315	39.68/12.315

Two-dimensional ^{15}N-$^{13}C\alpha$ Correlation	
MAS spinning speed (Hz)	11111
acquisition time (t2/t1) [ms]	10.4/6.08
carrier frequency (t2/t1) [ppm]	55/120
CP total contact time [μs]	1000
CP number of contacts	4
CP delay between contacts [ms]	100
CP rf field strength ($^{1}H/^{15}N$) [kHz]	49.6/38.5
CP pulse shape (^{1}H)	Linear (100-80%)
SPECIFIC-CP contact time [ms]	2.5
SPECIFIC-CP rf field strength ($^{15}N/^{13}C\alpha$) [kHz]	27/16
SPECIFIC-CP pulse shape (^{13}C)	tan (100-90%)
^{1}H decoupling rf field strength (SPINAL64) [kHz]	100
recycle delay [s]/number of acquisitions	2/7168
spectral width (F2/F1) [kHz]	50/3.125

Three-dimensional HnNCa (^{1}H-^{15}N DC / ^{15}N CS / $^{13}C\alpha$ CS)	
MAS spinning speed (Hz)	11111
acquisition time (t3/t1/t2) [ms]	10.46/1.26/3.52
carrier frequency ($^{1}H/^{13}C/^{15}N$) [ppm]	7/55/120
CP total contact time [μs]	1000
CP number of contacts	4
CP delay between contacts [ms]	100
CP rf field strength ($^{1}H/^{15}N$) [kHz]	49.6/38.5
CP pulse shape (^{1}H)	Linear (100-80%)
Z-filter [ms]	5
SPECIFIC-CP contact time [ms]	2.5
SPECIFIC-CP rf field strength ($^{15}N/^{13}C\alpha$) [kHz]	27/16
SPECIFIC-CP pulse shape (^{13}C)	tan (100-90%)
$R18^{7}_{1}$ pulse lengh rf field strength [kHz]	100
$R18^{7}_{1}$ ^{1}H carrier frequency [ppm]	9
^{1}H decoupling rf field strength (SPINAL64) [kHz]	100
recycle delay [s]/number of acquisitions	2/1216
spectral width (F3/F1/F2) [kHz]	50/5.55/3.125

Three-dimensional HnNCo (^{1}H-^{15}N DC / ^{15}N CS / $^{13}C'$ CS)	
MAS spinning speed (Hz)	11111
acquisition period (t3/t1/t2) [ms]	10.46/1.26/3.52
carrier frequency ($^{1}H/^{13}C\alpha/^{13}C'/^{15}N$) [ppm]	7/55/174/120
CP total contact time [μs]	1000

CP number of contacts	4
CP delay between contacts [ms]	100
CP rf field strength (^{1}H/^{15}N) [kHz]	49.6/38.5
CP pulse shape (^{1}H)	linear (100-80%)
Z-filter [ms]	5
SPECIFIC-CP contact time [ms]	2.5
SPECIFIC-CP rf field strength (^{15}N/^{13}C') [kHz]	27/38
SPECIFIC-CP pulse shape (^{13}C)	tan (100-90%)
$R18^{7}_{1}$ pulse lengh rf field strength [kHz]	100
$R18^{7}_{1}$ ^{1}H carrier frequency [ppm]	9
^{1}H decoupling rf field strength (SPINAL64) [kHz]	100
recycle delay [s]/number of acquisitions	2/2144
spectral width (F3/F1/F2) [kHz]	50/5.55/3.125

Three-dimensional HcCxCx (^{1}H-^{13}C DC / ^{13}C CS / ^{13}C CS)

MAS spinning speed (Hz)	13889
acquisition period (t3/t1/t2) [ms]	10/1.368/2.28
carrier frequency (^{1}H/^{13}Cα/^{13}CX/^{15}N) [ppm]	7/55/100/120
CP total contact time [μs]	320
CP number of contacts	4
CP delay between contacts [ms]	15
CP rf field strength (^{1}H/^{15}N) [kHz]	64/50
CP pulse shape (^{1}H)	linear (100-90%)
$R18^{7}_{1}$ pulse lengh rf field strength [kHz]	125
$R18^{7}_{1}$ ^{1}H carrier frequency [ppm]	7
DARR mixing time [ms]	20
^{1}H decoupling rf field strength (SPINAL64) [kHz]	100
recycle delay [s]/number of acquisitions	2/208
spectral width (F3/F1/F2) [kHz]	50/13.889/41.667

[a]**Abbreviations.** DC: dipolar coupling; CS: chemical shift; CP: cross polarization; MAS: magic angle spinning; DARR: dipolar assisted rotational resonance; PDSD: proton driven spin diffusion; rf: radio frequency; SPECIFIC-CP: spectrally induced filtering in combination with CP; SPINAL: small phase incremental alternation.

Supplementary Table 2. Values of the isotropic chemical shifts and dipolar couplings measured for individual residues in MerF in 14-o-PC liposomes.

Residue	^{15}N chemical shift (ppm)	^{13}Cα chemical shift (ppm)	^{13}C' chemical shift (ppm)	^{1}H-^{15}N dipolar coupling (kHz)	^{1}H-^{13}Cα dipolar coupling (kHz)
K5	120.90	58.78	176.70	10.82	15.6
T6	121.66	65.62	173.63	-3.87	3.2
L7	124.02	56.09	176.32	16.66	10.8
L8	122.08	56.18	175.82	16.90	0.6
R9	120.75	56.59	176.26	9.07	17.7
V10	119.30	64.09	175.99	7.13	11.9
S11	120.48	61.55	174.79	15.09	10.7
I12	125.38	63.85	176.98	16.75	2.0
I13	122.45	63.91	175.22	13.77	14.9
T15	120.57	66.15	174.67	17.73	8.4
T16	120.30	65.95	173.33	6.34	15.9
L17	123.25	56.29	175.94	8.71	13.3
V18	120.68	64.84	176.24	15.38	15.2
A19	120.35	53.88	177.01	15.42	13.1
L20	119.22	55.89	177.09	13.57	12.9
S21	116.93	57.96	172.15	11.85	12.3
S22	121.91	59.27	172.44	18.52	7.6
F23	120.76	56.22	175.11	7.25	6.5
T24	119.53	63.38	174.14	15.34	13.8
V26	120.73	65.46	175.44	12.96	10.9
L27	120.38	56.18	177.36	18.71	7.1
V28	120.42	66.37	174.36	14.89	12.7
I29	121.96	63.70	176.32	11.96	12.9
L30	122.40	56.79	175.82	15.62	1.6
L31	118.64	56.70	177.53	17.29	0.9
V33	123.00	65.95	174.23	16.51	15.3
V34	123.38	65.16	176.16	15.38	1.7
L36	121.01	55.89	177.20	12.20	15.1
S37	119.22	59.90	174.23	10.82	13.7
A38	125.19	53.06	178.02	18.25	8.9
L39	118.06	55.15	174.84	19.01	5.4
T40	104.52	59.98	171.37	18.27	14.4
Y42	120.78	57.31	172.92	1.65	2.6
L43	123.03	56.50	174.78	1.23	13.8
D44	121.32	56.50	174.78	3.46	14.8
Y45	120.64	59.78	174.01	-1.57	14.6
V46	120.49	60.05	173.03	-1.18	1.6
L47	120.99	56.70	176.32	16.31	9.0
L48	122.02	57.80	174.67	14.91	11.8
A50	119.13	54.68	177.69	12.89	9.8
L51	122.78	57.57	176.65	17.24	6.0
A52	123.87	53.73	178.02	12.29	16.2
I53	120.07	63.30	176.10	13.67	0.5
F54	117.59	60.21	175.96	17.94	14.6
I55	121.88	64.70	176.87	14.69	13.4
L57	121.97	56.25	176.05	15.24	1.6
T58	121.37	66.34	173.46	16.95	0.2
I59	122.49	63.40	175.99	15.33	11.1
Y60	120.95	60.00	174.89	15.29	15.2
A61	119.91	54.64	178.13	12.20	10.9
I62	122.48	64.20	176.21	15.97	2.8
Q63	118.55	55.74	176.98	13.77	13.7
R64	120.75	56.66	176.37	12.49	5.6
K65	120.97	57.10	176.76	14.26	17.0
R66	121.03	56.30	175.88	8.04	3.3
Q67	122.08	54.94	174.56	14.60	10.7
A68	125.73	51.18	176.50	7.06	3.1

D69	119.35	53.15	174.90	-4.20	2.3

Supplementary Table 3. The ranges of the chemical shift and dipolar couplings of leucine residues with respect to all residues in MerF. The limited ranges of isotropic chemical shifts illustrate the advantage of using dipolar coupling to resolve signals from the same types of amino acids.

	Leucine residues	All residues excluding Glycines	Leucine span percentage
^{15}N chemical shift (ppm)	118.06 to 124.02	104.52-125.73	28%
^{13}Cα chemical shift (ppm)	55.15 to 57.80	51.18 to 66.37	17%
^{13}C' chemical shift (ppm)	174.67 to 177.52	171.37 to 178.13	42%
^{1}H-^{15}N dipolar coupling (kHz)	1.23 to 19.01	1.23 to 19.01	100%
^{1}H-^{13}Cα dipolar coupling (kHz)	0.6 to 15.1	0.2 to 17.7	83%

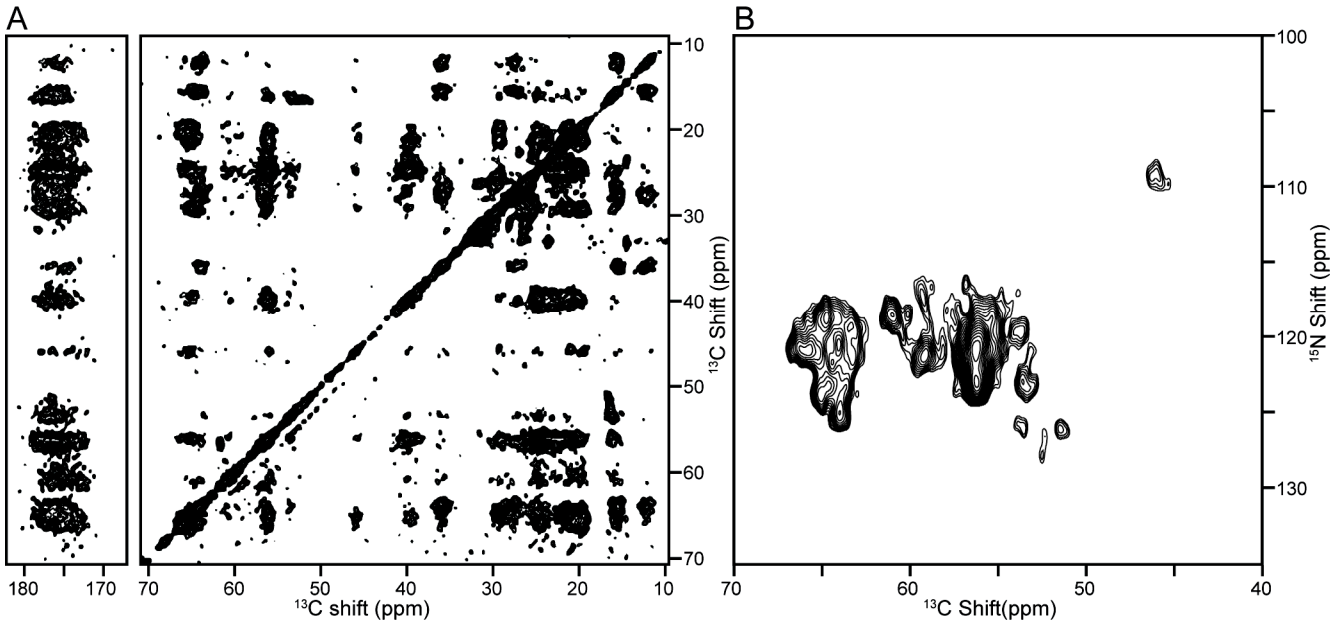

Supplementary Figure 2. Two-dimensional MAS spectra of uniformly $^{13}C/^{15}N$ labeled MerF in 14-o-PC proteoliposomes at 25°C: A. Homonuclear $^{13}C/^{13}C$ spin-exchange correlation spectrum with 200ms DARR mixing. B. Heteronuclear $^{13}C/^{15}N$ correlation spectrum.

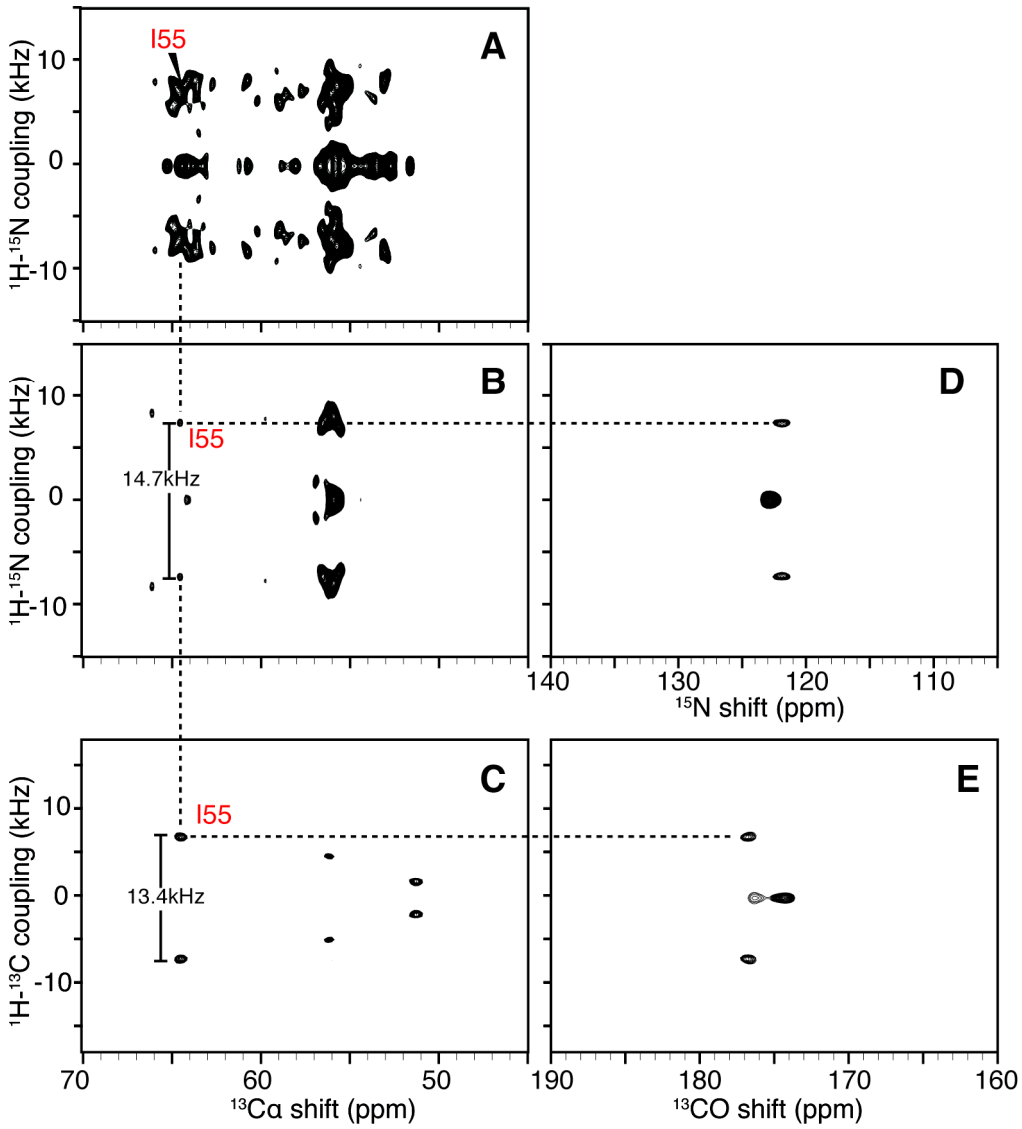

Supplementary Figure 3. Examples of spectroscopic data for residue I55 obtained from MAS solid-state NMR spectra of uniformly ^{13}C/^{15}N labeled MerF in 14-o-PC proteoliposomes at 25°C: A. Two-dimensional ^{1}H-^{15}N DC/^{13}C shift separated local field (SLF) spectrum. B. and D. Two-dimensional ^{1}H-^{15}N DC/^{13}Cα shift and ^{1}H-^{15}N DC/^{15}N shift SLF planes selected from a three-dimensional HnNCa spectrum at the ^{15}N shift frequency of 120.7 ppm and the ^{13}Cα shift frequency of 64.6 ppm. C. and E. Two-dimensional ^{1}H-^{13}Cα DC/^{13}Cα shift and ^{1}H–^{13}Cα DC/^{13}C' shift SLF planes selected from a three-dimensional HcCxCx spectrum at the 13C' shift frequency of 176.8 ppm and the ^{13}Cα shift frequency of 64.1 ppm. All spectral planes are associated with residue I55. The dashed line traces the correlations among the resonance frequencies. The DC frequencies in the spectra correspond to the rotary resonance recoupling at n=2 of the motionally averaged powder pattern[17].

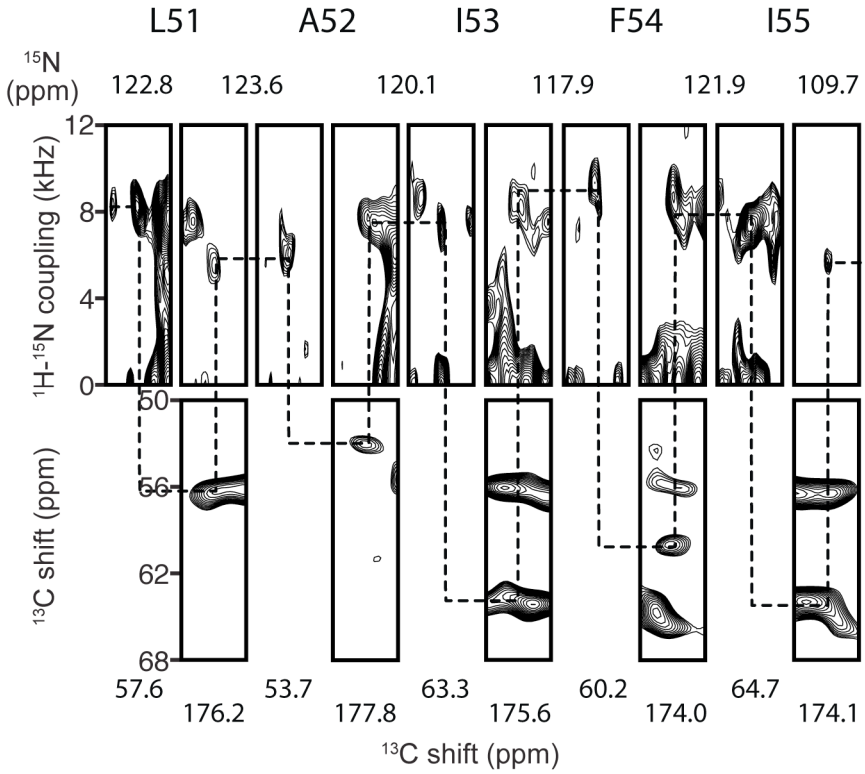

Supplementary Figure 4. Representative strip plots for residues L51-I55 of uniformly $^{13}C/^{15}N$ labeled MerF in 14-o-PC proteoliposomes at 25 °C. Dashed lines are provided as guides through the backbone resonance walk. For each residue, the connectivities proceed through the sequence of HnNCa, HcCxCx and HnNCo experiments.

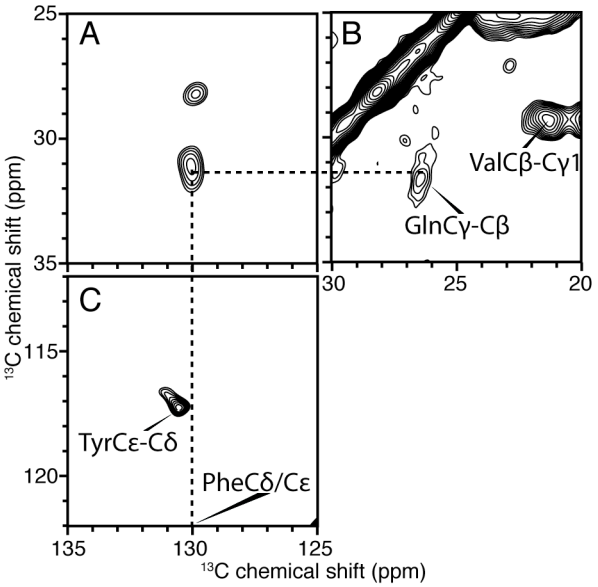

Supplementary Figure 5. Interhelical long-range distance restraints for MerF structure determination. A. Two-dimensional ^{13}C-^{13}C correlation spectrum obtained with 200ms DARR mixing for through-space correlation of atoms separated by < 5.5 Å[20]. A distinct cross-peak between Phe Cδ or Cε and Gln Cγ is marked. B. and C. Two-dimensional ^{13}C-^{13}C spectrum obtained with 50ms PDSD mixing for intra-residual correlation. B. Gln Cγ has a unique chemical shift frequency that can be distinguished from Val, Pro and Lys signals. C. The chemical shift of Phe Cδ is well separated from that of Tyr Cδ, which rules out the assignment of the cross-peak in Panel A. to be between Y60 and Gln. Therefore, the crosspeak in Panel A. can only be between Gln Cγ and Phe Cδ or Cε. Since both Q63 and Q67 are in the same helix as F54 and are separated by nine or more residues, they are more than 10 Å apart in space. Consequently, a cross-peak is only feasible between F23 and Q63 or Q67. Many other inter-helical cross-peaks are possibly observed in the spectrum of 200ms DARR mixing; however, only this peak can be unambiguously assigned due to the unique chemical shifts of both Gln Cγ and Phe aromatic ring atoms.

Supplementary Table 4. NMR and refinement statistics for MerF.

Experimental NMR restraints	
Total dihedral angle restraints	
phi	79
psi	78
Total dipolar coupling (DC) restraints	
^{1}H-^{15}N DC	59
^{1}H-^{13}C DC	58
Total distance restraints	
inter-helical long-range	1
short-range	48

Structure statistics[a]	
Violations (mean and s.d.)	
Dihedral angle restraints (°)	0.000 ± 0.000
^{1}H-^{15}N DC restraints (kHz)	0.000 ± 0.000
^{1}H-^{13}CA DC restraints (kHz)	3.600 ± 0.966
Deviations from idealized geometry	
Bond lengths (Å)	0.004 ± 0.000
Bond angles (°)	0.546 ± 0.024
Impropers (°)	0.449 ± 0.030
Average pairwise r.m.s.d. (Å)	
Heavy	2.58 ± 0.31
Backbone	1.48 ± 0.27

Ramachandran plot statistics[b]	
residues in most favoured regions (%)	87.990 ± 2.162
residues in additional allowed regions (%)	11.590 ± 2.260
residues in generously allowed regions (%)	0.420 ± 0.676
residues in disallowed regions (%)	0.000 ± 0.000

[a]Evaluated for 10 lowest energy structures out of a total 200 calculated structures for residues 5-69 of MerF.

[b]Evaluated with the program PROCHECK[21].

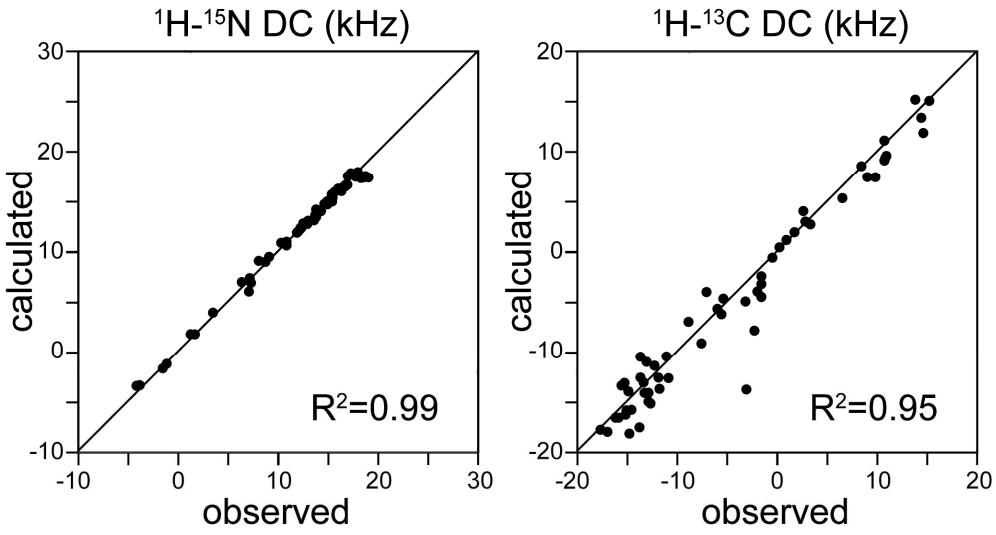

Supplementary Figure 6. Plots of the correlations between observed and back-calculated values of ^{1}H-^{15}N and ^{1}H-^{13}C dipolar coupling used to calculate the structure of MerF in phospholipid bilayers. The R^2 correlation coefficients are shown for each type of restraint.

Reference:

(1) Howell, S. C.; Mesleh, M. F.; Opella, S. J. *Biochemistry* **2005**, *44*, 5196.

(2) De Angelis, A. A.; Howell, S. C.; Nevzorov, A. A.; Opella, S. J. *J. Am. Chem. Soc.* **2006**, *128*, 12256.

(3) Lu, G. J.; Son, W. S.; Opella, S. J. *J. Magn. Reson.* **2011**, *209*, 195.

(4) Son, W. S.; Park, S. H.; Nothnagel, H. J.; Lu, G. J.; Wang, Y.; Zhang, H.; Cook, G. A.; Howell, S. C.; Opella, S. J. *J. Magn. Reson.* **2012**, *214*, 111.

(5) Lu, G. J.; Park, S. H.; Opella, S. J. *J. Magn. Reson.* **2012**, *220*, 54.

(6) Park, S. H.; Casagrande, F.; Chu, M.; Maier, K.; Kiefer, H.; Opella, S. J. *Biochim. Biophys. Acta-Biomembr.* **2012**, *1818*, 584.

(7) Park, S. H.; Das, B. B.; Casagrande, F.; Tian, Y.; Nothnagel, H. J.; Chu, M.; Kiefer, H.; Maier, K.; De Angelis, A. A.; Marassi, F. M.; Opella, S. J. *Nature* **2012**, *491*, 779.

(8) Delaglio, F.; Grzesiek, S.; Vuister, G. W.; Zhu, G.; Pfeifer, J.; Bax, A. *J. Biomol. NMR* **1995**, *6*, 277.

(9) Goddard, T. D. K., D. G.. SPARKY 3; University of California, San Francisco.

(10) Fung, B. M.; Khitrin, A. K.; Ermolaev, K. *J. Magn. Reson.* **2000**, *142*, 97.

(11) Bloembergen, N. *Physica* **1949**, *15*, 386.

(12) Frey, M. H.; Opella, S. J. *J. Am. Chem. Soc.* **1984**, *106*, 4942.

(13) Takegoshi, K.; Nakamura, S.; Terao, T. *Chem. Phys. Lett.* **2001**, *344*, 631.

(14) Tang, W.; Nevzorov, A. A. *J. Magn. Reson.* **2011**, *212*, 245.

(15) Pines, A.; Gibby, M. G.; Waugh, J. S. *J. Chem. Phys.* **1973**, *59*, 569.

(16) Baldus, M.; Petkova, A. T.; Herzfeld, J.; Griffin, R. G. *Mol. Phys.* **1998**, *95*, 1197

(17) Zhao, X.; Edén, M.; Levitt, M. H. *Chem. Phys. Lett.* **2001**, *342*, 353.

(18) Levitt, M. H. *Symmetry-Based Pulse Sequences in Magic-Angle Spinning Solid-State NMR*; John Wiley & Sons, Ltd, 2007.

(19) Carravetta, M.; Edén, M.; Zhao, X.; Brinkmann, A.; Levitt, M. H. *Chem. Phys. Lett.* **2000**, *321*, 205.

(20) Zech, S. G.; Wand, A. J.; McDermott, A. E. *J. Am. Chem. Soc.* **2005**, *127*, 8618.

(21) Laskowski, R.; Rullmann, J. A.; MacArthur, M.; Kaptein, R.; Thornton, J. *J. Biomol. NMR* **1996**, *8*, 477.